



Novel 2,4-difluorophenyl-functionalized arylamine as hole-injecting/hole-transporting layers in organic light-emitting devices

Zhanfeng Li, Zhaoxin Wu^{*}, Bo Jiao, Peng Liu, Dongdong Wang, Xun Hou

Key Laboratory of Photonics Technology for Information of Shaanxi Province, and Key Laboratory for Physical Electronics and Devices of the Ministry of Education, School of Electronic and Information Engineering, Xi'an Jiaotong University, Xi'an 710049, People's Republic of China

ARTICLE INFO

Article history:

Received 3 November 2011

In final form 8 December 2011

Available online 16 December 2011

ABSTRACT

Novel 2,4-difluorophenyl-functionalized triphenylamine and its dimer, namely tris(2',4'-difluorobiphenyl-4-yl)-amine (3FT) and N^4,N^4,N^4,N^4 -tetrakis-(2',4'-difluorobiphenyl-4-yl)-biphenyl-4,4'-diamine (4FDT), have been synthesized and characterized. The device with the configuration of ITO/4FDT/Alq₃/LiF/Al yields maximum current efficiency of 4.3 cd/A. Moreover, with 4FDT as the hole-injecting layer, the maximum efficiency and luminance of the device was further improved to be 5.0 cd/A and 19880 cd/m², respectively. The good performance of devices with 4FDT as HTL or HIL was attributed to the incorporation of the strong electron-withdrawing fluorinated substituents into the arylamine moiety, which reduced holes mobility of HTL and HIL and then balanced the injected carriers in devices.

© 2011 Elsevier B.V. All rights reserved.

1. Introduction

Triarylamine and its derivatives have long been exploited as hole-transport layers (HTLs) for organics-based (opto)electronic devices such as organic light-emitting devices (OLEDs), organic solar cells (OSCs), or organic thin-film transistors (OTFTs) [1–3], and their range of application is continuously widening. In many applications, hole-transport materials are conventionally combined with other organic molecules or/and with metallic electrodes; it is therefore, important for substituted triarylamines to tune their electronic structure in order to control the relative frontier orbital energies, that is, the energies of the highest occupied molecular orbital (HOMO) or the lowest unoccupied molecular orbital (LUMO). It is well-known that the charge balancing control of electroluminescence (EL) devices, namely the reduction of the hole mobility of the hole-transporting materials (HTMs) in matching the electron mobility of electron transporting materials (ETMs), is effective in achieving high EL efficiency [4–7]. Previous studies had shown that the incorporation of the strong electron-withdrawing fluorinated substituents into hole-transporting (p-type) semiconductors, which may contribute to tuning the electronic properties, and altering charge transport properties [8–14]. In particular, electron-withdrawing groups, such as –CN, –F and –CF₃, in direct conjunction with the electron-donor N atoms of the well-known hole-transport material N,N' -bis(tolyl)- N,N' -diphenyl-1,1'-biphenyl-4,4'-diamine (TPD), lower the HOMO levels and the hole mobility and tune the molecular properties, such as solubility or stability [15–18].

However, fluorine-functionalized arylamine as HTLs in OLEDs is still scarce, and further studies are still desirable.

In this Letter, we reported the synthesis and characterization of two novel fluorinated triphenylamine (TPA) and its dimer (DTPA), 3FT and 4FDT being the adducts of TPA and DTPA cores with three and four 2,4-difluorophenyl peripheral moieties, respectively, in which electron-withdrawing fluorine atoms were introduced into the periphery of the aryl substituents of (D)TPA moieties to lower the HOMO levels and reduce the hole-transport. The new 2,4-difluorophenyl-functionalized (D)TPA, 3FT and 4FDT, exhibited good thermal stabilities, proper HOMO/LUMO energy levels and the hole-transporting ability, which were suitable for HIL or HTL in OLEDs. The typical bilayer devices with the fluorinated (D)TPA as HTLs yield maximum current efficiency of 3.9 cd/A for 3FT and 4.3 cd/A for 4FDT, which exceed that of the prototypical N,N' -bis-(1-naphthalenyl)- N,N' -bis-phenyl-(1,1'-biphenyl)-4,4'-diamine (NPB)-based device (3.8 cd/A) with the same device structure. Furthermore, by using 4FDT as HIL, high-performance OLED was achieved with a maximum luminance around 19880 cd/m² and maximum efficiency above 5.0 cd/A.

2. Experimental section

2.1. Materials and instruments

The manipulation involving air-sensitive reagents was performed under an inert atmosphere of dry nitrogen. Other reagents in the scheme were used as received from commercial sources. Absorption (UV) spectra were recorded on a Hitachi UV 3010 spectrophotometer. PL spectra were recorded on a Horiba Jobin Yvon

^{*} Corresponding author. Fax: +86 29 82664867.

E-mail address: zhaoxinwu@mail.xjtu.edu.cn (Z. Wu).

Fluoromax-4 spectrophotometer. Decomposition temperatures (T_d) were obtained using TG209C thermal gravimetric analysis (TGA) with a heating rate of $20\text{ }^\circ\text{C min}^{-1}$ and glass transition temperatures (T_g) were determined with a differential scanning calorimeter (DSC, TA instruments DSC200PC) at a heating rate of $10\text{ }^\circ\text{C min}^{-1}$ under a N_2 atmosphere. To measure the fluorescence quantum yields (Φ_{PL}), degassed solutions of the compounds in CH_2Cl_2 were prepared. The concentration was adjusted so that the absorbance of the solution would be lower than 0.1. The excitation was performed at 334 nm, and quinine sulfate in 1.0 M H_2SO_4 solution, which has $\Phi_{\text{PL}} = 0.56$, was used as a standard [19]. Cyclic voltammetry was performed using a Princeton Applied Research model 273 A potentiostat at a scan rate of 100 mV s^{-1} . All experiments were carried out in a three-electrode compartment cell with a Pt-sheet counter electrode, a glassy carbon working electrode and a Pt-wire reference electrode. The supporting electrolyte used was 0.1 M tetrabutylammonium perchlorate ($[\text{Bu}_4\text{N}][\text{ClO}_4]$) solution in dry acetonitrile. The cell containing the solution of the sample (1 mM) and the supporting electrolyte was purged with a nitrogen gas thoroughly before scanning for its oxidation and reduction properties. Ferrocene was used for potential calibration in each measurement. All the potentials were reported relative to ferrocene-ferrocenium (Fc/Fc^+) couple, whose oxidation potential was +0.22 V relative to the reference electrode. The oxidation and reduction potentials were determined by taking the average of the anodic and cathodic peak potentials. The HOMO and LUMO values were estimated by using the following general equation: $E_{\text{HOMO}} = -(qE_{\text{ox}} + 4.8)\text{ eV}$; $E_{\text{LUMO}} = E_{\text{HOMO}} - E_{\text{g}}^{\text{opt}}$ [20], which were calculated using the internal standard ferrocene value of -4.8 eV with respect to the vacuum level [21].

2.2. Synthesis

2.2.1. Tris(2',4'-difluorobiphenyl-4-yl)amine (3FT)

Tris(4-bromophenyl)amine (2.41 g, 5 mmol), 2,4-difluorophenylboronic acid (2.84 g, 18 mmol), $\text{Pd}(\text{PPh}_3)_4$ (0.58 g, 0.5 mmol), aqueous Na_2CO_3 (2.0 M, 15 mL), ethanol (10 mL) and toluene (30 mL) were mixed in a flask under nitrogen. The mixture was heated to reflux and maintained at this temperature overnight. When the reaction was completed (judging from thin-layer chromatography), water was added to quench the reaction. Then, the products were extracted with CH_2Cl_2 . The organic layer was collected, dried over anhydrous MgSO_4 and evaporated under vacuum. The solid was absorbed on silica gel and purified by column chromatography using light petrol ether/ethyl acetate (20:1) as the eluent to give 3FT as a white solid (2.44 g, 85%). $^1\text{H NMR}$ (CDCl_3 , 400 MHz): δ 6.88–6.97 (m, 6H), 7.22–7.25 (t, $J = 8.4\text{ Hz}$, 6H), 7.39–7.44 (m, 9H). Anal. Calcd for $\text{C}_{36}\text{H}_{21}\text{NF}_6$: C, 74.35%; H, 3.64%; N, 2.41%. Found: C, 74.31%; H, 3.01%; N, 2.77%. MS: m/z 581.1592 [M^+] (Calcd: 581.5491).

2.2.2. N^4,N^4,N^4,N^4 -tetrakis(4-bromophenyl)biphenyl-4,4'-diamine (2)

To a 100 mL round-bottom flask were added 2.44 g, 5 mmol N^4,N^4,N^4,N^4 -tetraphenylbiphenyl-4,4'-diamine (DTPA) and 3.56 g, 20 mmol NBS. Chloroform (30 mL) was added, and the solution was stirred at room temperature (RT) for 1 h. And then 12.5 mL of acetic acid were added, and the solution was stirred for further 6.5 h at RT. The product was extracted with diethyl ether, washed with water and brine twice and then the organic extract dried over anhydrous sodium sulfate. After solvent evaporation, the crude product was recrystallized from chloroform and hexane to afford white solid (3.55 g, 88%). $^1\text{H NMR}$ (CDCl_3 , 400 MHz): δ 6.99–7.00 (d, $J = 8.8\text{ Hz}$, 8H), 7.11–7.13 (d, $J = 8.4\text{ Hz}$, 4H), 7.37–7.40 (d, $J = 8.8\text{ Hz}$, 8H), 7.46–7.49 (d, $J = 8.8\text{ Hz}$, 4H). Anal. Calcd for $\text{C}_{36}\text{H}_{24}\text{N}_2\text{Br}_4$: C, 53.77%; H, 3.01%; N, 3.48%. Found: C, 51.71%; H, 2.32%; N, 3.66%.

2.2.3. N^4,N^4,N^4,N^4 -tetrakis(2',4'-difluorobiphenyl-4-yl)-biphenyl-4,4'-diamine (4FDT)

The experimental procedure for N^4,N^4,N^4,N^4 -tetrakis(2',4'-difluorobiphenyl-4-yl)-biphenyl-4,4'-diamine (4FDT) was similar to that for the synthesis of 3FT described above. A white solid was obtained in 78% yield. $^1\text{H NMR}$ (CDCl_3 , 400 MHz): δ 6.91–7.00 (m, 12H), 7.24–7.28 (t, 8H), 7.41–7.47 (m, 12H), 7.54–7.56 (d, $J = 8.8\text{ Hz}$, 4H). Anal. Calcd for $\text{C}_{60}\text{H}_{36}\text{N}_2\text{F}_8$: C, 76.92%; H, 3.87%; N, 2.99%. Found: C, 76.59%; H, 3.42%; N, 3.29%. MS: m/z 936.2759 [M^+] (Calcd: 936.9285).

2.3. OLEDs fabrication and characterizations

The devices were fabricated by conventional vacuum deposition of the organic layers, LiF and Al cathode onto an ITO-coated glass substrate under a base pressure lower than $1 \times 10^{-3}\text{ Pa}$ at the rates of 0.04, 0.025, 0.5 nm/s, respectively. The thickness of each layer was determined by a quartz thickness monitor. The effective size of the OLED was 14 mm^2 . The voltage–current (V – I), voltage–current density (V – J) and voltage–brightness (V – L) as well as the current density–current efficiency (J – η) curve characteristics of devices were measured with a Keithley 2602 and Source Meter. The detailed devices fabrication can be found in previous paper in our group [22].

3. Results and discussion

3.1. Synthesis

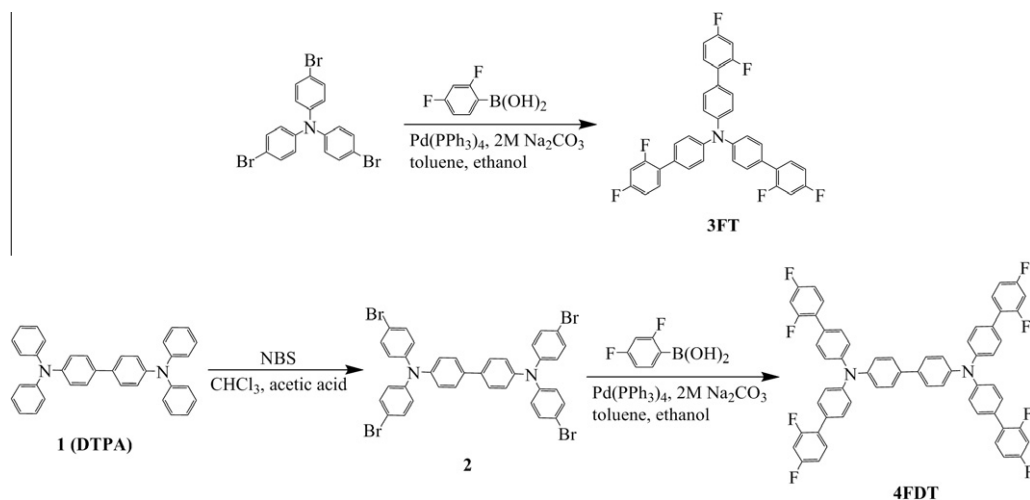
Scheme 1 shows the chemical structures and the synthetic routes of tris(2',4'-difluorobiphenyl-4-yl)-amine (3FT) and N^4,N^4,N^4,N^4 -tetrakis-(2',4'-difluorobiphenyl-4-yl)-biphenyl-4,4'-diamine (4FDT) examined in this study. The syntheses of N^4,N^4,N^4,N^4 -tetraphenylbiphenyl-4,4'-diamine (DTPA) was carried out in 89% yield by using a palladium-catalyzed Buchwald–Hartwig amination reaction between 4,4'-dibromobiphenyl and diphenylamine [23,24]. Bromination of **1** (DTPA) by means of NBS in glacial acetic acid at ambient temperature gave **2** in 88% yield [25]. Suzuki coupling reactions of 2,4-difluorophenylboronic acid with **1** and **2** were catalyzed by $\text{Pd}(\text{PPh}_3)_4$ [26], giving 3FT and 4FDT, respectively, in good yields (ca. 78–85%). All the reaction intermediates and final products were characterized by ^1H nuclear magnetic resonance ($^1\text{H NMR}$), mass spectrometry (MS) and element analysis. The results are in good agreement with proposed structures. The synthesized compounds could dissolve in common organic solvents, such as toluene, chloroform and THF, etc.

3.2. Thermal properties

The thermal properties of 3FT and 4FDT were evaluated by TGA and DSC. The onset temperatures for 5% weight loss (T_d) in nitrogen of 4FDT was $513\text{ }^\circ\text{C}$, which is significantly higher than that of the most widely used hole-transporting material (e.g., $410\text{ }^\circ\text{C}$ for NPB). The glass-transition temperature (T_g) of 4FDT was found to be $113\text{ }^\circ\text{C}$ in the second heating scan, after rapid cooling of the melted sample, while those of the hole-transporting material NPB and the hole-injecting/transporting material *m*-MTDATA are 98 and $75\text{ }^\circ\text{C}$, respectively [27]. The thermal transitions T_g , T_m and T_d are 69, 181 and $374\text{ }^\circ\text{C}$, respectively, for 3FT. Therefore, thermal analyses indicate that 4FDT with high T_d and T_g would be used as a good active layer in OLED devices.

3.3. Photophysical properties

Figure 1 shows the normalized absorption and photoluminescence (PL) spectra of 3FT and 4FDT dilute solutions in dichloromethane.



Scheme 1. Synthesis of compounds 3FT and 4FDT.

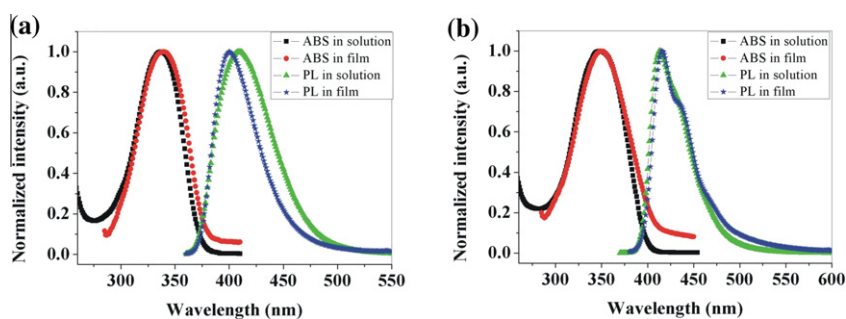


Figure 1. Absorption and fluorescence spectra of 3FT (a) and 4FDT (b) in solution and in film.

Table 1

Optical, thermal and electrochemical properties of the compounds.

Compounds	λ_{abs} CH_2Cl_2 (nm)	λ_{em} CH_2Cl_2 (nm)	λ_{em} film (nm)	Φ_{PL}^a CH_2Cl_2	E_g^b (eV)	E_{ox}^c (V)	HOMO ^d (eV)	LUMO ^e (eV)	T_g/T_d ($^{\circ}\text{C}$)
3FT	338	411	399	0.49	3.28	0.48	-5.3	-2.0	69/374
4FDT	349	413	416	0.56	3.06	0.31, 0.43	-5.1	-2.1	113/513

^a Determined in CH_2Cl_2 using quinine sulfate ($\Phi_{\text{PL}} = 0.56$ in 1.0 M H_2SO_4 solution) as standard.^b Calculated from the onset of absorption in thin film.^c Measured vs. Fc/Fc^+ in CH_3CN .^d Estimated from onset oxidation voltages with reference to ferrocene (4.8 eV vs. vacuum).^e Calculated from HOMO and optical band gap.

ane and its as-cast thin film at room temperature. In the UV–visible spectra, the absorption bands observed around 340 nm in solution can be attributed to π – π^* transitions of the conjugated aromatic rings. The UV–visible absorption maximum in the solution state was 338 nm for 3FT, while the peak of 4FDT was red-shifted by 11 nm, suggesting that the latter was more conjugated than the former. From the onset of the film absorption spectrum, the energy band gap (E_{gs}) of 3FT and 4FDT in thin film were calculated to be 3.28 and 3.06 eV, respectively (Table 1). And the two compounds could be applied to HTL due to no absorption at visible light region.

3FT and 4FDT in the solid state displayed a bright blue emission peak with maxima at ca. 399 and 416 nm, respectively (Figure 1). It is worth noting that the photoluminescence spectra of the compounds in films are almost identical to those in solution, which indicates the prearrangement of two fluorine atoms at the 2,4-positions in the phenyl ring of each arm in 3FT and 4FDT efficiently

suppresses intimate intermolecular packing in the condensed solid state, whereas the main characteristics of the spectra remain unchanged [28].

3.4. Electrochemical properties

The redox behaviors of the compounds 3FT and 4FDT were evaluated by cyclic voltammetry (CV) experiments at ambient temperature; see Figure 2. During the oxidation scan in acetonitrile, both compounds 3FT and 4FDT show reversible oxidation processes. 3FT displays a reversible oxidation wave, which is a one-electron process attributed to the oxidation of the triphenylamine core while the highly extended 4FDT exhibits two sequential one-electron processes, corresponding to removal of two electrons from the DTPA unit. The oxidation potential of 3FT relative to ferrocene is 0.48 V, which is significantly higher than that of tri(biphenyl-4-

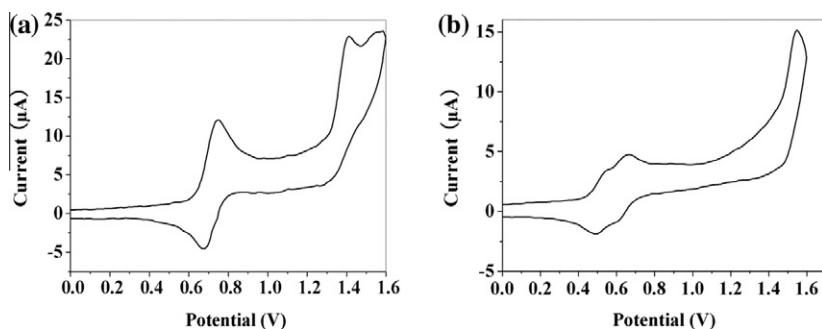


Figure 2. Cyclic voltammogram of 3FT (a) and 4FDT (b) in CH_3CN , Pt wire used as reference electrode.

yl)amine (TBA) (0.18 V vs. Fc) [29]. The difference between 3FT and TBA in oxidation potential was attributed to the strongly electron-withdrawing fluorine substituent on the aryl substituents of TPA electron donor [15,30]. The DTPA core significantly lowers the oxidation potential, as evident by the 0.31 V value for 4FDT vs. 0.48 V for 3FT. The reason is that the longer the conjugated aryl core, which can better stabilize the radical cation(s), the lower the oxidation potential is. Similarly to most other triphenylamine compounds, 3FT and 4FDT have the HOMO (-5.1 and -5.3 eV, respectively) close to the work function of indium tin oxide (ITO) and thus allows efficient hole injection from the ITO. Thus a hole-injecting/hole-transport capacity for 3FT and 4FDT was expected. The LUMO determined by the difference of HOMO and optical energy gap was tabulated in Table 1. The LUMO energy values of 3FT and 4FDT were calculated to be -2.0 and -2.1 eV, respectively. And the high-lying LUMO energy level of the compounds 3FT and 4FDT suggested that they possess good electron-blocking abilities as well.

3.5. Quantum chemical calculations

The geometry and the HOMO and LUMO energy levels of 3FT and 4FDT were optimized using density functional theory (DFT) method with the B3LYP hybrid functional and the 6-31G(d) on carbon and hydrogen, and all calculations described here were carried out using the GAUSSIAN 98 program [31]. As illustrated in Figure 3, the core triphenylamine (TPA) group in 3FT shows the three-dimensional propeller structure, and difluorophenyl groups act as the linear arms. This geometry could result in good solution processability. The HOMO distributes in the whole molecule with higher density on the TPA unit, whereas the LUMO is located predominantly on the two arms of the molecule. Similarly, the HOMO orbitals of 4FDT are localized on the amine moieties, that is DTPA unit, and the LUMO orbital in 4FDT reside on two separated difluorobiphenyl arms of the molecule. The broad distribution of the HOMO should be good for the hole transport through the molecules when both 3FT and 4FDT are used as hole-injecting/hole-transporting materials in the OLEDs.

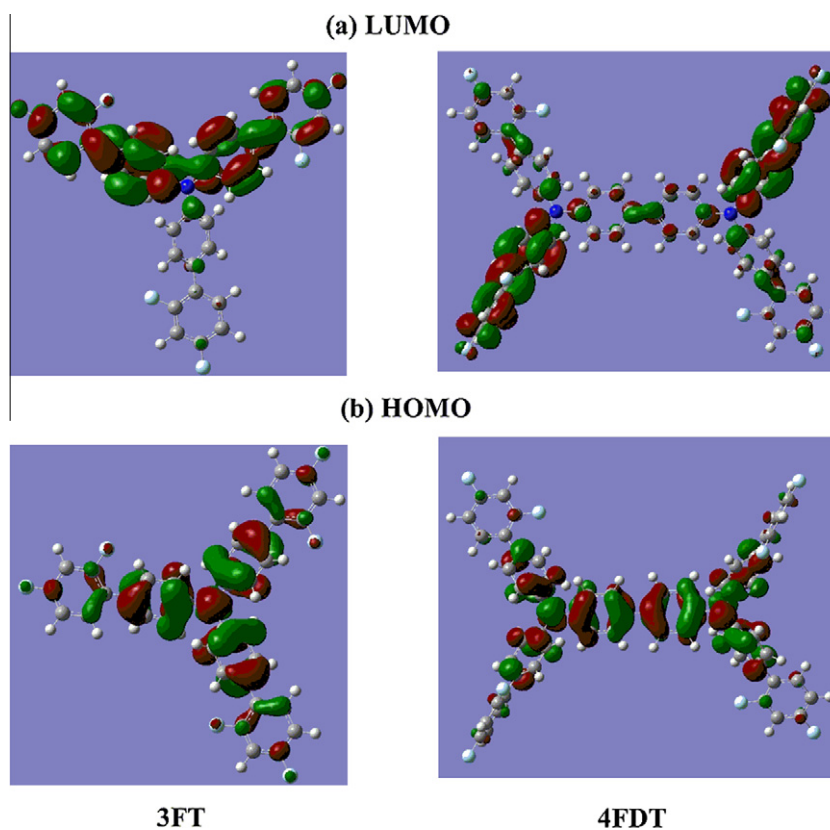


Figure 3. Calculated spatial distributions of LUMO and HOMO of 3FT and 4FDT.

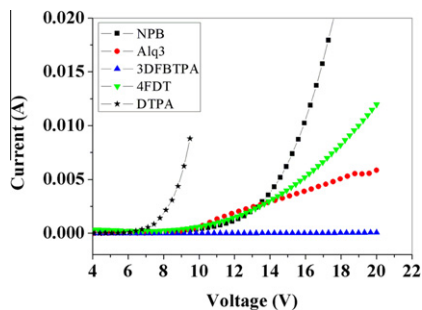


Figure 4. Current–voltage for the hole-only devices, ITO/NPB, DTPA, 3FT or 4FDT (100 nm)/Ag (80 nm), and the electron-only device, ITO/Alq₃ (100 nm)/LiF (1 nm)/Al (70 nm).

As shown in Table 1, the experimental HOMO and LUMO are in excellent agreement with the calculated values (−5.5 and −5.3 eV for the HOMO, and −1.5 eV for the LUMO of 3FT and 4FDT, respectively).

3.6. Electroluminescent properties

The incorporation of the strong electron-withdrawing fluorinated substituents into hole-transporting triphenylamine and its dimer moiety in 3FT and 4FDT is expected to lower the hole mobility. To evaluate the hole-transport of 3FT and 4FDT, we fabricated and characterized the hole-only devices, ITO/NPB, DTPA, 3FT or 4FDT (100 nm)/Ag (80 nm), and the electron-only device, ITO/Alq₃ (100 nm)/LiF (1 nm)/Al (70 nm). In Figure 4, it was found that the following sequence for the current at a given applied voltage in single-layer devices: DTPA > NPB >> 4FDT > Alq₃ > 3FT. This result shows that the incorporation of the strong electron-withdrawing fluorinated substituents into hole-transporting materials could

tune charge transport properties. When the electron-withdrawing fluorinated substituent to electron-donor moiety ratio is equal to 2, 4FDT exhibits lower mobility than regular DTPA and NPB and the hole-current of 4FDT-based hole-only device is quit close to electron-current of the Alq₃-based electron-only device at applied voltages lower than 16 V. Moreover, the lowest hole-transport of 3FT might be due to the fact that there is only one electron-donor moiety and that the ratio of electron-withdrawing fluorinated substituent to electron-donor moiety is 3 in the molecule [4,5]. Therefore, 4FDT was suitable to be HTL for the more balanceable carrier-transport in the device.

Based on the unique properties of 3FT and 4FDT including good thermal stabilities, optical properties, proper HOMO/LUMO energy levels and the hole-transporting nature of (D)TPA derivatives, both are expected to be potential hole-transporting materials in electroluminescent devices. We fabricated the typical two-layer device with the structure of ITO/3FT or 4FDT (60 nm)/Alq₃ (60 nm)/LiF(1 nm)/Al (70 nm), where Alq₃ is electron transporting and light-emitting layer. For comparison, a typical and widely used hole transporter NPB has been chosen and a conventional ITO/NPB (60 nm)/Alq₃ (60 nm)/LiF(1 nm)/Al (70 nm) device was fabricated under the same conditions. In Figure 5, for the 4FDT-based device, the highest efficiency reached 4.3 cd/A, much higher than that of the device with NPB as the HTL (3.8 cd/A). The better performance of 4FDT-based device was attributed to the more balanceable injected carriers in the device than that in the NPB-based device, which was also shown in Figure 4. As for the 3FT-based device, the current density and luminance are the poorer than those of NPB-based device, although its maximum current efficiency is 3.9 cd/A, and almost equal to NPB-based device (3.8 cd/A). This poorer performance of the 3FT-based device may resulted from the less injected and transported holes than electrons in devices, as shown in Figure 4.

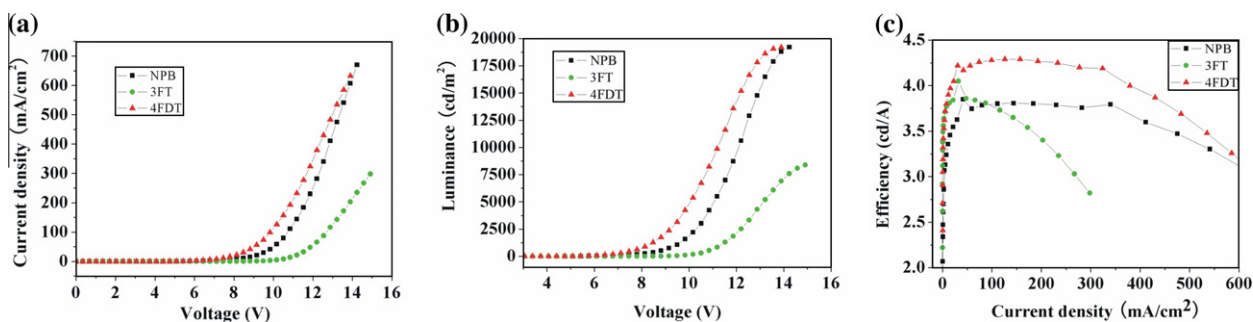


Figure 5. Current–density–voltage curves (a), Luminance–voltage curves (b) and Efficiency–current–density curves (c) for the ITO/NPB, 3FT or 4FDT (60 nm)/Alq₃ (60 nm)/LiF(1 nm)/Al (70 nm) devices.

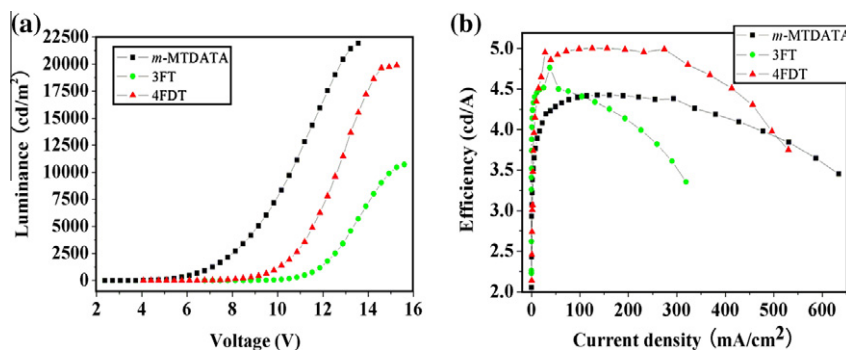


Figure 6. Luminance–voltage curves (a) and Efficiency–current–density (b) curves for the ITO/*m*-MTDATA, 3FT or 4FDT (40 nm)/NPB(20 nm)/Alq₃ (60 nm)/LiF(1 nm)/Al (70 nm) devices.

Since the HOMO energy levels of 4FDT are similar to those of *m*-MTDATA (5.1 eV), which is well-known and commonly used hole-injecting material, both compounds 3FT and 4FDT were introduced as a hole-injecting layer (HIL). In order to compare the performance of the devices, *m*-MTDATA was selected for control HIL material. Each device was fabricated with the following structure: ITO/HIL (40 nm)/NPB (20 nm)/Alq₃ (60 nm)/LiF (1 nm)/Al (70 nm), where NPB is hole-transport layer; Alq₃ is electron-transport and light-emitting layer; and HIL is 3FT, 4FDT or *m*-MTDATA. Figure 6 shows the voltage–luminance and efficiency–current–density characteristics for the devices. For the 3FT and 4FDT-based devices, the current efficiency surpassed those of the *m*-MTDATA-based device. Especially for the 4FDT-based device, the highest efficiency and maximum luminance were 5.0 cd/A and 19880 cd/m² respectively. The improved EL performance can be attributed to the greater charge balance and better exciton confinement within the emission layer.

4. Conclusions

In summary, two fluorinated (D)TPA molecules 3FT and 4FDT, have been designed, synthesized and applied as hole-injecting/hole-transporting materials in organic light-emitting devices (OLEDs). It was found that the introduction of the strong electron-withdrawing fluorine substituents to the periphery of the aryl substituents of D(TPA) moieties can reduce the hole-transport and lower the HOMO levels, and the hole-transport of 4FDT matched well with electron-transport of Alq₃. The fluorinated compound 4FDT, used in a typical bilayer OLED, exhibits a better performance with maximum current efficiency of 4.3 cd/A, which is higher than that of the NPB-based device (3.8 cd/A) with the same device structure. In addition, the device performance with 4FDT as the HIL could be further improved in ITO/4FDT (40 nm)/NPB (20 nm)/Alq₃ (60 nm)/LiF (1 nm)/Al (70 nm) device, and the current efficiency and maximum luminance were 5.00 cd/A and 19880 cd/m², respectively. In sight of its better thermal stability ($T_g = 113\text{ }^\circ\text{C}$) than that of NPB ($T_g = 98\text{ }^\circ\text{C}$), and the much better performance of 4FDT-based device, 4FDT is promising hole-injecting/hole-transporting material for applications in organic light-emitting devices.

Acknowledgements

This work was supported by National Natural Science Foundation of China (Grant 61 106 123).

References

- [1] Y. Shirota, H. Kageyama, Chem. Rev. 107 (2007) 953.
- [2] Z.-J. Ning, H. Tian, Chem. Commun. (2009) 5483.
- [3] Z.-J. Zhao et al., Chem. Commun. 47 (2011) 6924.
- [4] S.-L. Tao et al., Chem. Mater. 21 (2009) 1284.
- [5] Q. Zhang, J.-S. Chen, Y.-X. Cheng, L.-X. Wang, D.-G. Ma, X.-B. Jing, F.-S. Wang, J. Mater. Chem. 14 (2004) 895.
- [6] J.-Y. Li, C.-W. Ma, J.-X. Tang, C.-S. Lee, S.-T. Lee, Chem. Mater. 17 (2005) 615.
- [7] Q.-X. Tong et al., Chem. Mater. 19 (2007) 5851.
- [8] M.-S. Jang, S.-Y. Song, H.-K. Shim, Polymer 41 (2000) 5675.
- [9] J.-S. Reddy, T. Kale, G. Balaji, A. Chandrasekaran, S. Thayumanavan, J. Phys. Chem. Lett. 2 (2011) 648.
- [10] D.J. Crouch et al., Chem. Mater. 17 (2005) 6567.
- [11] Y. Jin, J. Kim, S. Lee, J.Y. Kim, S.H. Park, K. Lee, H. Suh, Macromolecules 37 (2004) 6711.
- [12] A. Facchetti, M.-H. Yoon, C.L. Stern, H.E. Katz, T.J. Marks, Angew. Chem. Int. Ed. 42 (2003) 3900.
- [13] D.J. Crouch, P.J. Skabara, M. Heeney, I. McCulloch, S.J. Coles, M.B. Hursthouse, Chem. Commun. (2005) 1465.
- [14] S. Ando, J.-I. Nishida, E. Fujiwara, H. Tada, Y. Inoue, S. Tokito, Y. Yamashita, Chem. Mater. 17 (2005) 1261.
- [15] E. Bellmann, S.E. Shaheen, R.H. Grubbs, S.R. Marder, B. Kippelen, N. Peyghambarian, Chem. Mater. 11 (1999) 399.
- [16] J. Cornil et al., J. Phys. Chem. A 105 (2001) 5206.
- [17] M. Malagoli, M. Manoharan, B. Kippelen, J.L. Brédas, Chem. Phys. Lett. 354 (2002) 283.
- [18] J.-L. Maldonado et al., Chem. Mater. 15 (2003) 994.
- [19] J.N. Demas, G.A. Crosby, J. Phys. Chem. 75 (1971) 991.
- [20] A.J. Bard, L.R. Faulkner, Electrochemical Methods—Fundamentals and Applications, Wiley, New York, 1984.
- [21] H. M. Koeppe, H. Wendt, H. Strehlow, Z. Elektrochem. 64 (1960) 483.
- [22] B. Jiao, Z.X. Wu, Y. Dai, D.D. Wang, X. Hou, J. Phys. D: Appl. Phys. 42 (2009) 205108.
- [23] B.E. Koene, D.E. Loy, M.E. Thompson, Chem. Mater. 10 (1998) 2235.
- [24] T. Yamamoto, M. Nishiyama, Y. Koie, Tetrahedron Lett 39 (1998) 2367.
- [25] W.Z. Yuan et al., Adv. Mater. 22 (2010) 2159.
- [26] N. Miyaura, A. Suzuki, Chem. Rev. 95 (1995) 2457.
- [27] Y. Shirota et al., Appl. Phys. Lett. 65 (1994) 807.
- [28] L. Zhao et al., Org. Electron. 9 (2008) 649.
- [29] A. Higuchi, K. Ohnishi, S. Nomura, H. Inada, Y. Shirota, J. Mater. Chem. 2 (1992) 1109.
- [30] F. Babudri, G.M. Farinola, F. Naso, R. Ragni, Chem. Commun. (2007) 1003.
- [31] M.J. Frisch et al., R. A. Gaussian 98, Gaussian, Inc., Pittsburgh, PA, 1998.